MECHANICAL, THERMAL AND OPTICAL PROPERTIES OF NEW CHLOROANTIMONITE GLASSES IN THE Sb_2O_3–$PbCl_2$–AgCl SYSTEM

D. YEZLI[1], *M. LEGOUERA*[1], *R. EL ABDI*[2], *M. POULAIN*[3], *V. BURGAUD*[2]

[1] *Département de Génie Mécanique, Université du 20 aout 1955, Skikda, Algérie;*

[2] *IPR, Département Mécanique &Verres, Université de Rennes1, Rennes cedex, France;*

[3] *UMR Sciences Chimiques, Université de Rennes1, Rennes cedex, France*

New chloroantimonite glasses were obtained in the Sb_2O_3–$PbCl_2$–AgCl ternary system. Thermal, optical and mechanical properties were studied. The silver chloride concentration was increased at the expense of antimony oxide according to the following composition rules: $(80-x)Sb_2O_3$–$20PbCl_2$–$xAgCl$; $(70-x)Sb_2O_3$–$30PbCl_2$–$xAgCl$. Depending on AgCl content, Vickers micro-hardness varied between 110 MPa and 140 MPa. Elastic moduli were measured by ultrasonic velocity. The optical transmission range extended from 400 nm in the visible spectrum to 7 μm in the infrared spectrum. The refractive index was close to 2. Glass transition temperature measured by DSC ranged from 250 to 290°C. It was noticed that the glass transition temperature decreased as AgCl substitute for Sb_2O_3 and the more stable system was with 20% $PbCl_2$ in the $(80-x)Sb_2O_3$–$20PbCl_2$–$xAgCl$.

Keywords: *glasses; chemical synthesis; differential scanning calorimetry (DSC); mechanical properties; optical properties.*

Glass forming ability of antimony sesquioxide Sb_2O_3 has been predicted by Zachariasen [1] and confirmed by several authors [2, 3]. While vitreous Sb_2O_3 has been reported, multicomponent glasses have been characterized either in pure oxide systems or in oxyhalide [4–7] and oxysulphide systems [8]. Not surprisingly, large amounts of Sb_2O_3 could be incorporated in silicates and phosphate glasses [9–11]. Antimonite glasses free of classic vitrifiers appear attractive for their extended infrared transmission range [3, 5, 8], their large refractive index (> 2) [5] and their non-linear optical properties [12–13]. In this respect they are compared to tellurite glasses that have been widely studied. The chlorides of the metal halide may be incorporated into the glasses of heavy oxides to obtain a very large subfamily [5]. This work is centred upon new chloroantimonite glasses associating antimony oxide and lead and silver halides. Following the pioneering work of Dubois and Portier [5], numerous glass forming systems have been reported [14–18].

While alkali antimonite glasses have been studied [3, 15], more numerous and more stable glasses were identified, especially by incorporating a third component in the binary Sb_2O_3–$PbCl_2$ glass.

In this paper we focus on the optical and mechanical properties of glasses in the Sb_2O_3–$PbCl_2$–AgCl ternary system.

Experimental. *Glass synthesis.* Chemical reagents used for this study were 99.9% Sb_2O_3 (Acros organics), 99% $PbCl_2$ + (Hichem) and 99.9% AgCl (Alfa Aesar).

The main physical properties of these starting materials are given in Table 1.

Glass preparation was carried out using the classic processing steps of melting, fining, cooling, casting and annealing. The calculated amount of starting materials was thoroughly mixed in an agate mortar, and then introduced into a silica tube. Silica was

Corresponding author: R. EL ABDI, e-mail: relabdi@ univ-rennes1.fr

not an ideal material for this glass synthesis as it slowly reacts with melted glass. However it is a better choice than platinum or gold, both of which may form alloys if oxido-reduction reactions result in metallic particles. In this case, the crucible was destroyed.

Table 1. Mechanical properties of used materials

Components	ρ, g/cm^3	M, g/mol	HV, MPa	V, cm^3/mol
PbCl$_2$	5.7	278.1	138…140	48.78
AgCl	5.4	143.32	10…12	26.54
Sb$_2$O$_3$	5.75	291.4	65…68	50.79

After melting, fining was achieved at room atmosphere at around 850°C. Then the melt was rapidly cooled down to approximately 600°C and poured onto a brass mould preheated to 250°C, which is around the glass transition temperature T_g. After solidification, the sample was set in an oven at T_g for the thermal homogenization for the removal of the thermally induced stress. After a few hours, the oven was turned off to ensure homogenous cooling.

Physical measurements. Characteristic temperatures – T_g for glass transition, T_x for onset of crystallization, and T_c for exotherm maximum were measured by differential scanning calorimetry using a DSC Q20 set-up from TA instruments.

The density was measured by the Archimedean method using CCl$_4$ as buoyancy liquid. The molar volume was calculated from the following equation [19]:

$$V = \sum x_i \cdot M_i / \rho, \tag{1}$$

where x_i is the molar fraction of the i element, M_i is the molar weight of the i element and ρ is material density. The molar weight of the glass M_g is expressed as $M_g = \sum x_i \cdot M_i$; this depends directly on the chemical formulation.

Microhardness was measured using a Matuzawa Vmt 75 set-up with 50 N loading charge and 10 s indentation time.

Elastic moduli were measured by ultrasonic velocity using a "Parametric 5800" device and an oscilloscope "model 54502".

Optical transmission was recorded in the UV-visible range using a Perkin Elmer spectrophotometer between 300 nm and 3000 nm. For infrared transmission a Bruker Tensor 37 Fourier transformed spectrometer was used between 400 cm^{-1} and 4000 cm^{-1}.

Results and discussion. *Glass formation.* The starting point of our study was the binary glass Sb$_2$O$_3$–PbCl$_2$ reported by Dubois et al. [5]. A third component was added to form a ternary system. From our results, the glass forming area in this system is shown in Fig. 1. The limits of the vitreous domain correspond to small spheres, roughly 1 mm in diameter. Larger and thicker samples could be obtained for the non-limiting composition. Antimony oxide was the main component while the PbCl$_2$ concentration did not
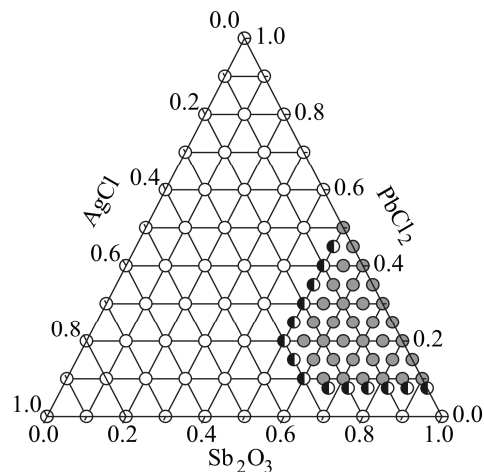

Fig. 1. Compositional limits for glass formation in Sb$_2$O$_3$–PbCl$_2$–AgCl$_2$ system: ● – glass; ◑ – ceramic glass; ○ – ceramic.

exceed 40 mol.% and maximum AgCl content was less than 30 mol.%. Note that no binary glass was observed in the Sb_2O_3–AgCl system. The vitreous state was assessed by visual inspection and confirmed by thermal analysis. Samples of several millimetres thick were prepared for optical and mechanical measurements. It appears that the most stable compositions correspond to the 20% molar concentration of lead chloride.

Density and molar volume. The density was measured for two series of glasses defined by the following composition rules: $(80-x)Sb_2O_3$–$20PbCl_2$–$xAgCl$ and $(70-x)Sb_2O_3$–$30PbCl_2$–$xAgCl$.

This corresponds to the substitution of Sb_2O_3 by AgCl. Collected data provided information on the influence of silver chloride on physical properties. Fig. 2 reports the changes of density and molar volume versus AgCl concentration.

Both density and molar volume decreased as AgCl replaced Sb_2O_3. The molar weight corresponds to the chemical formula: αSb_2O_3–$\beta PbCl_2$–$\gamma AgCl$ with $\alpha + \beta + \gamma = 100$.

The density was measured for the two series of glasses, which makes it possible to evaluate the influence of the composition. The influence of Sb and Ag on density values is illustrated by Fig. 2. For each curve, the lead chloride content was kept constant. The density decrease resulting from the Sb/Ag substitution could be expected insofar as the Ag^+ ion is larger and lighter than that of the Sb^{3+}, while chlorine anions are also larger than oxygen anions. This results in a smaller number of ions per unit volume. The conjugation of these two factors (size and atomic weight) accounts for density reduction.

Density and molar volume follow almost quasi-linear slopes especially for the $(70-x)Sb_2O_3$–$30PbCl_2$–$xAgCl$ system.

Our measurements allow a comparison of glasses with 20% and 30 mol.% lead chloride, corresponding to the substitution of antimony oxide by lead chloride. When $x = 5$ or 10 (AgCl) the density (e.g. $x = 5$, $\rho = 5.36$ g/cm^3) of the $(80-x)Sb_2O_3$–$20PbCl_2$–$xAgCl$ glass system (Fig. 2a) is smaller than that (e.g. $x = 5$, $\rho = 5.42$ g/cm^3) of the $(70-x)Sb_2O_3$–$30PbCl_2$–$xAgCl$ glass system (Fig. 2b). However, when x increases to 15 and is as much as 25, the density (e.g. $x = 25$, $\rho = 5.22$ g/cm^3) of the $(70-x)Sb_2O_3$–$30PbCl_2$–$xAgCl$ glass system is much smaller compared to that (e.g. $x = 25$, $\rho = 5.33$ g/cm^3) of the $(80-x)Sb_2O_3$–$20PbCl_2$–$xAgCl$ glass system. This means the glass density decreases as the lead component increases.
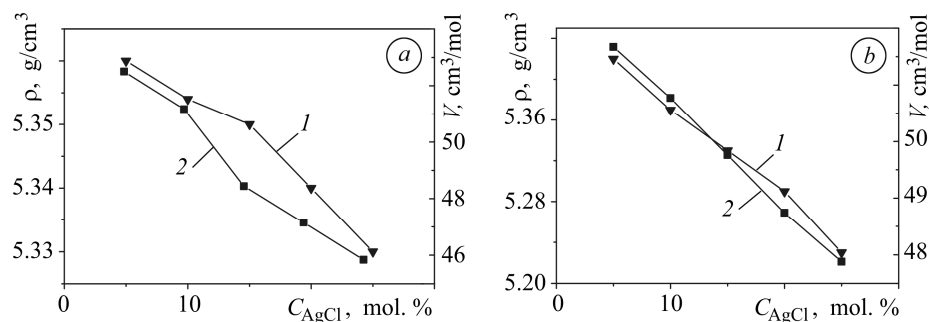

Fig. 2. Change of the density and molar volume according to AgCl concentration: a – $(80-x)Sb_2O_3$–$20PbCl_2$–$xAgCl$; b – $(70-x)Sb_2O_3$–$30PbCl_2$–$xAgCl$) system. *1* – density; *2* – molar volume.

Thermal properties. The characteristic temperatures of the selected glasses were measured. They included temperatures of glass transition T_g, onset of crystallization T_x and exothermic maximum T_c.

The T_x–T_g difference makes a qualitative criterion of the stability versus devitrification. Their variation as a function of AgCl concentration is shown in Fig. 3. The ge-

neral trend was that T_g decreased as AgCl substituted Sb_2O_3. This substitution increased the Cl/O ratio. As the AgCl bond is weaker than the Sb–O bond, the resistance to thermal motion decreased and consequently T_g was smaller.

As this is currently observed in multicomponent glasses, there is no direct relationship between T_g changes and glass stability. While the T_g value depends mainly on bond strength and glass structure, crystallization temperature is ruled by nucleation and crystal growth. Both processes are temperature dependent, but they cannot be simply correlated to chemical composition. For this reason the development of a stable glass composition against devirification remains largely empirical.
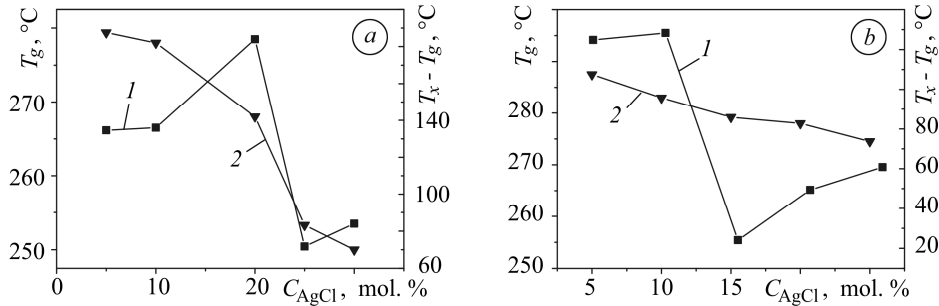

Fig. 3. Change of the Tg and stability based on AgCl of $(80–x)Sb_2O_3–20PbCl_2–xAgCl$ (*a*); $(70–x)Sb_2O_3–30PbCl_2–xAgCl$ system (*b*). *1* – $T_x–T_g$; *2* – T_g.

Table 2 gives the detailed composition of the studied glass samples. The DSC scans of Fig. 4 suggest that glasses far from the limiting compositions were very stable insofar as the crystallization peak was hardly visible at the DSC heating rate (20 K/min).

Table 2. Composition of samples studied

Samples	$(80–x)Sb_2O_3–20PbCl_2–xAgCl$	Samples	$(70–x)Sb_2O_3–30PbCl_2–xAgCl$
D_1	$75Sb_2O_3–20PbCl_2–5AgCl$	E_1	$65Sb_2O_3–30PbCl_2–5AgCl$
D_2	$70Sb_2O_3–20PbCl_2–10AgCl$	E_2	$60Sb_2O_3–30PbCl_2–10AgCl$
D_3	$60Sb_2O_3–20PbCl_2–20AgCl$	E_3	$55Sb_2O_3–30PbCl_2–15AgCl$
D_4	$55Sb_2O_3–20PbCl_2–25AgCl$	E_4	$50Sb_2O_3–30PbCl_2–20AgCl$
D_5	$50Sb_2O_3–20PbCl_2–30AgCl$	E_5	$45Sb_2O_3–30PbCl_2–25AgCl$
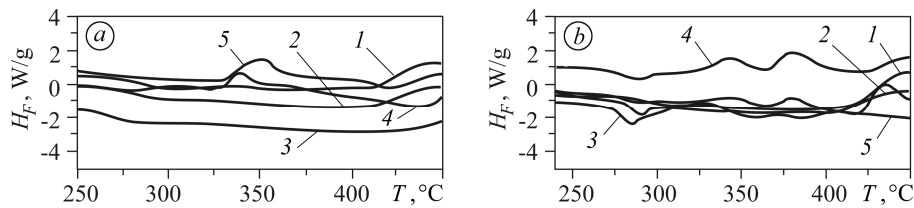
Fig. 4. DSC curves for $(80–x)Sb_2O_3–20PbCl_2–xAgCl$ (*a*: *1* – D_1; *2* – D_2; *3* – D_3; *4* – D_4; *5* – D_5); $(70–x)Sb_2O_3–30PbCl_2–xAgCl$ system (*b*: *1* – E_1; *2* – E_2; *3* – E_3; *4* – E_4; *5* – E_5).

Vickers microhardness and Young's modulus. To characterize the hardness and the deformation mode of the glass surface, the indentation hardness technique was used. When a sharp indenter, such as a Vickers indenter, was loaded onto a material, a residual surface impression was observed after unloading, and the material hardness was generally estimated from the projected area of the impression. The deformation was dependent on the applied load, the temperature and the load time.

Indentation experiments were performed with a Vickers diamond indenter. The Vickers diamond pyramid hardness was determined in practice by measuring the diagonal length of the indentation produced by the penetration of a square-based pyramid having an angle of 136° between opposite pyramid faces. The hardness number HV (in MPa) was given by the equation:

$$HV = \frac{0.1891F}{d^2},$$

(2)

F is the applied load, and d is the average length of the square diagonal left by the indenter.

Although the diagonal d, in Eq. (2) was obtained by measurement after the removal of the load, it was known that the change in the lengths of the diagonals upon unloading was very small [20] and almost insignificant when compared to the diagonal length itself.

The Vickers hardness was calculated for each sample using the average residual area of 9 indentations.

The microhardness was measured for the two sample systems as shown in Fig. 5.

For the studied glasses, the initial hardness value was approximately equal to $140\,\text{N/mm}^2$ and decreased according to the AgCl concentration. This decrease can reach 22% and the insertion of more and more AgCl into the glasses network. This confirms the fact that AgCl is able to soften the glasses.

But this is not the same case for the $PbCl_2$ that leads to the decrease of the glass hardness. Increasing $PbCl_2$ from 20 mol.% to 30 mol.% lowers the microhardness from $HV = 130$ MPa to 110 MPa (Fig. 5).

One can note that the microhardness was also connected to the dilatometric softening point. The glass microhardness systematically decreased according to the softening temperature which depended on the transition glass temperature T_g. Thus, respective changes of microhardness and glass transition temperature were similar.
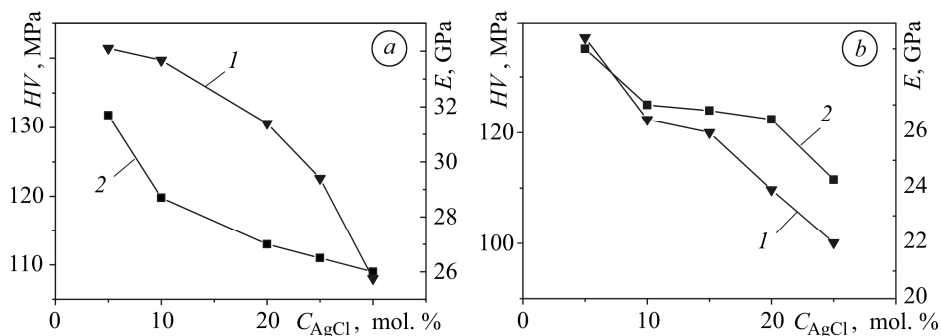

Fig. 5. Change of the microhardness HV (curve *1*) and Young's modulus E (curve *2*) based on AgCl: $(80–x)Sb_2O_3–20PbCl_2–xAgCl$ (*a*); $(70–x)Sb_2O_3–30PbCl_2–xAgCl)$ system (*b*).

Flaking. Tenacity represents the resistance of the material against defect or crack propagation. It is expressed in $MPa\sqrt{m}$.

When the percentage of AgCl increases, one obtains soft glasses with an increase of the tenacity. Indeed for 20% AgCl (Fig. 6*a*, *c*) radial cracks are visible and start from the top of each corner of the Vickers indenter footprint. These cracks are between 0.1 and 0.2 mm. The increase of AgCl concentration (from 10 to 25%) makes a tough material and radial cracks disappeared (Fig. 6*b*, *d*).

One can note that one effect is the production of glass flakes which overlap towards the thinner part of the sample, which appear on either side of the footprint of the diamond indenter.
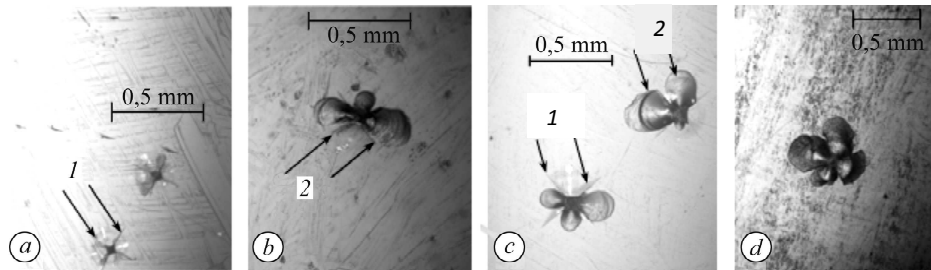
Fig. 6. Radial and lateral cracks for different molar concentrations of AgCl:
a – $70Sb_2O_3$–$20PbCl_2$–$10AgCl$; b – $55Sb_2O_3$–$20PbCl_2$–$25AgCl$; c – $60Sb_2O_3$–$30PbCl_2$–$10AgCl$;
d – $45Sb_2O_3$–$30PbCl_2$–$25AgCl$. 1 – radial cracks; 2 – lateral cracks.

Infrared and UV transmission. Fig. 7 shows the ultraviolet-visible transmission spectrum. A Perkin Elmer spectrophotometer was used on 2 mm thick samples. The level of the maximum transmission (about 65%) was due to a refractive index greater than 2, which caused the reflection losses. The base line of the E glass sample (Fig. 7, dotted line) is shifted towards a smaller transmission value because it contains physical defects that result in high scattering losses. These physical defects consist of "stones" and "cords" that are visible to the naked eye. They result from the processing conditions and lead to scattering losses that decrease as the wavelength increases.

The yellow color of antimony glasses reflects their limited ultraviolet transmission below 400 nm and partial blue absorption. This is due to the low gap band of the free electron pair of Sb (III).

In these glasses, infrared transmission is limited by chemical bond vibrations and their harmonics that create the multiphonon absorption edge.

A Bruker Tensor 37 Fourier transformed spectrometer was used for measurement of infrared transmission (2.5 μm to 25 μm) using 2 mm thick samples with parallel plane sections. Fig. 8 gives IR transmission for two samples of the studied systems. For clarity, the base line has been raised.

The main extrinsic absorption bands in these antimonite glasses are due to hydroxyls OH (3300 cm^{-1}), to Si–O bonds (1800 cm^{-1}) or to carbon dioxide (2400 cm^{-1}).
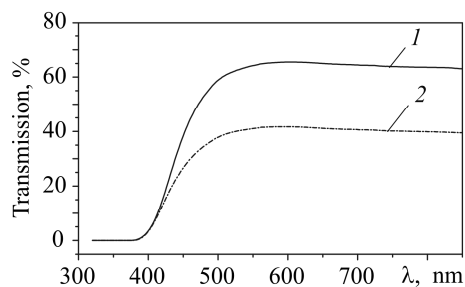

Fig. 7.

Fig. 8.

Fig. 7. UV-visible transmission spectrum: 1 – $D/60Sb_2O_3$–$20PbCl_2$–$20AgCl$;
2 – $E/55Sb_2O_3$–$30PbCl_2$–$15AgCl$.
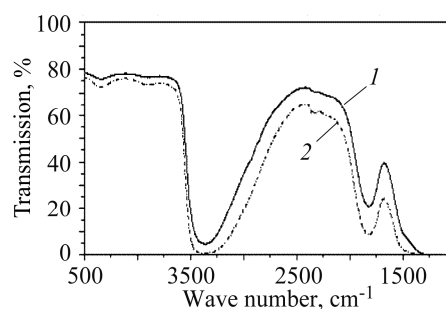
Fig. 8. Infrared transmission spectrum: 1 – $D/60Sb_2O_3$–$20PbCl_2$–$20AgCl$;
2 – $E/55Sb_2O_3$–$30PbCl_2$–$15AgCl$.

Influence of silver chloride on glass transparency. The increase of AgCl concentration (from 5% to 25%) in the system $(70–x)Sb_2O_3$–$30PbCl_2$–$xAgCl$ dims the obtained glasses (Fig. 9). The same phenomenon was observed for the second studied

system $(80–x)Sb_2O_3–20PbCl_2–xAgCl$. This exemplifies the photosensitivity of these glasses: under light illumination monovalent silver is reduced by trivalent antimony to silver chloride, leading to metallic silver nanoparticles.
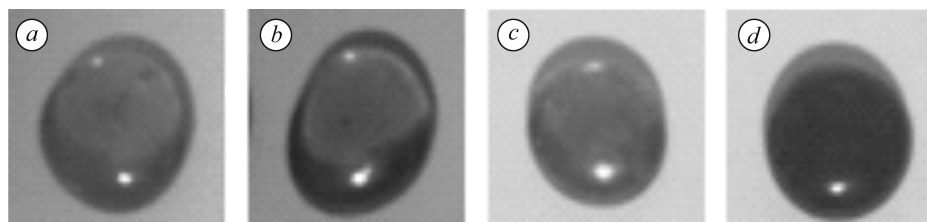

Fig. 9. Color change versus AgCl concentration for the $(70–x)Sb_2O_3–30PbCl_2–xAgCl$ system: $a – 5\%$; $b – 10\%$; $c – 20\%$; $d – 25\%$.

CONCLUSION

Glass formation has been studied in the $Sb_2O_3–PbCl_2–AgCl$ ternary system. In this system two groups of glasses were prepared according to the following composition rules: $(80–x)Sb_2O_3–20PbCl_2–xAgCl$ and $(70–x)Sb_2O_3–30PbCl_2–xAgCl$. The increase of the molar concentration of AgCl led to the decrease of the molar volume and the glass density. Increasing $PbCl_2$ concentration gave the same effect. Similar variations were observed for the transition glass temperature according to AgCl and $PbCl_2$ concentrations. A practical observation was that the more stable system was with 20% of $PbCl_2$ in the $((80–x)Sb_2O_3–20PbCl_2–xAgCl)$ series. Young's modulus and microhardness behave in the same way and both decrease when the AgCl concentration increases. The larger values of hardness and Young's modulus were obtained in the previous system $(80–x)Sb_2O_3–20PbCl_2–xAgCl$, and the maximum was obtained for 5% AgCl concentration. Finally, this study showed the interest in AgCl which can produce optimized glasses for various applications.

РЕЗЮМЕ. Описано нові хлорантімонітові скла, отримані в потрійній системі $Sb_2O_3–PbCl_2–AgCl$. Подано результати дослідження їх теплових, оптичних і механічних властивостей. Вміст хлориду у складі цих матеріалів збільшено, що вплинуло на їх мікротвердість. Залежно від вмісту AgCl мікротвердість скла змінювалася в межах від 110 до 140 MPa. Оптичний діапазон пропускання збільшений з 400 nm у видимій області спектра до 7 μm в інфрачервоному спектрі. Показник заломлення ~2. Температура склування, виміряна методом диференційної сканівної калориметрії, коливалася в межах 250...290°C. Відмічено, що вона зменшується за заміни Sb_2O_3 AgCl і найстабільніша система з 20% $PbCl_2$ у склі $(80–x)Sb_2O_3–20PbCl_2–xAgCl$.

РЕЗЮМЕ. Описаны новые хлорантимонитовые стекла, полученные в тройной системе $Sb_2O_3–PbCl_2–AgCl$. Представлены результаты исследований их тепловых, оптических и механических свойств. Содержание хлорида в составе этих материалов увеличено, что повлияло на их микротвердость. В зависимости от содержания AgCl микротвердость стекла изменялась в пределах от 110 до 140 MPa. Оптический диапазон пропускания увеличен от 400 nm в видимой области спектра до 7 μm в инфракрасном спектре. Показатель преломления ~2. Температура стеклования, измеренная методом дифференциальной сканирующей калориметрии, колебалась в пределах 250...290°C. Отмечено, что она уменьшается в меру замены Sb_2O_3 AgCl и наиболее стабильная система с 20% $PbCl_2$ в стекле $(80–x)Sb_2O_3–20PbCl_2–xAgCl$.

1. *Zachariasen W. H.* The Atomic arrangement in glass // J. Chem. Soc. – 1932. – **54**. – P. 3841–3851.
2. *Winter A.* Glass formation // J. Am. Ceram. Soc. – 1957. – **40**. – P. 54–58.
3. *Winter A.* Transformation region of glass // J. Am. Ceram. Soc. – 1943. – **26**. – P. 189–200.
4. *Bednarik J. F. and Neely J. A.* A Single component antimony oxide glass and some of its properties // Glass Tech. Ber. – 1982. – **55**. – P. 126–129.

5. *New* oxyhalide glasses involving Sb_2O_3 / B. Dubois, H. Aomi, J. J. Videau, J. Portier, P. Haggenmuller // Mater. Res. Bull. – 1984. – **19**. – P. 1317–1323.

6. *Sahar M. R., Ahmed M. M., and Holland D.* The crystallisation of Sb_2O_3–$PbCl_2$–$ZnCl_2$ glasses // Phys. Chem. Glasses. – 1990. – **31**. – P. 126–131.

7. *Sahar M. R. and Holland D.* Chemical durability of oxychloride glasses // J. Non-Cryst. Solids. – 1992. – **140**. – P. 107–111.

8. *Zan L., Zhong J. S., and Luo Q. R.* New oxysulphide glasses from the Sb_2O_3–Sb_2S_3MxS system // J. Non-Cryst. Solids. – 1999. – **256**–**257**. – P. 396–399.

9. *Datta A., Giri A. K., and Chakravorty D.* Ac conduction in sol-gel derived glasses in the SiO_2–As_2O_3 system // Physic. Rev. – 1993. – **B 47**. – P. 16242–16246.

10. *Chowdari B.V. R. and Akhter S. K.* Studied of lithium phosphoantimonite glass system // Solid State Ionics. – 1987. – **25**. – P. 109–119.

11. *Akhter S. K.* Physical characterization of lithium phophoantimonite glass system // Solid State Ionics. – 1992. – **51**. – P. 305–310.

12. *Wang J. S., Vogel E. E., and Snitzer E.* Tellurite glass: a new candidate for fiber devices // Opt. Mater. – 1994. – **3**. – P. 187–203.

13. *Non-linear* optical bsoption of antimony and lead oxyhalide glasses / R. E. De Araujo, C. B. De Araujo, G. Poirier, M. Poulain, Y. Messaddeq // Appl. Phys. Lett. – 2002. – **81**. – P. 4694–4696.

14. *Poirier G., Poulain M. A., and Poulain M. J.* Effects of carbon, hydrocarbon and hydroxide impurties on pradseodymium doped arsenic sulfide based glass // J. Non-Cryst. Solids. – 2001. – **284**. – P. 117–122.

15. *New* alkali antimonite glass / M. T. Soltani, A. Boutarfaia, R. Makhloufi, M. Poulain // J. Phys. Chem. Solids. – 2003. – **64**. – P. 2307–2312.

16. *Legouera M., Kostka P., and Poulain M.* Glass formation in the Sb_2O_3–$ZnBr_2$ binary system // J. Phys. Chem. Solids. – 2004. – **65**. – P. 901–906.

17. *New* heavy metal oxide glasses based on Sb_2O_3 / M. T. Soltani, T. Djouama, A. Boutarfaia, M. Poulain // J. Optoelectron. Advanced Mater. Symposia. – 2009. – **1**. – P. 339–342.

18. *Glass* formation in the Sb_2O_3–$CdCl_2$–$SrCl_2$ binary system / M. Iezid, M. Legouera, F. Goumeindane, M. Poulain, V. Nazabal, R. Lebullenger // J. Non-Cryst Solids. – 2011. – **357**. – P. 2984–2988.

19. *Stevels J. M.* Progress in the Theory of the Physical Properties of Glasses. – New York: Elsevier, 1948. – 96 p.

20. *Application* of atomic force microscopy for microindentation testing / M. Petzold, J. Landgraf, M. Füting, J. M. Olaf // Thin Sol. Films. – 1995. – **264**. – P. 153–158.